Microphase and macrophase separation in blends with a two-block copolymer

B. Löwenhaupt and G. P. Hellmann*
Deutsches Kunststoff-Institut, Schlossgartenstrasse 6, D-6100 Darmstadt, Germany
(Received 18 December 1989; revised 16 May 1990; accepted 21 May 1990)

The miscibility behaviour of blends A/$\alpha\beta$ of a homopolymer A and a symmetric two-block copolymer $\alpha\beta$, where the chains A and the blocks α are chemically the same and immiscible with the blocks β, is analysed theoretically and experimentally. The blends are compared with corresponding blends A/$\alpha\beta'$, where the copolymer $\alpha\beta'$ is random. The styrene (S)/methyl methacrylate (MMA) model systems investigated consist of a copolymer P(S-*b*-MMA) (two-block) or P(S-*co*-MMA) (random) and a homopolymer PMMA of varying chain length. The process of phase separation during film casting at different temperatures was analysed by mean-field calculations, and the morphologies of the cast films were studied by transmission electron microscopy. The block copolymer blends exhibit both microphase and macrophase separation, which develop in two steps in the order microphase–macrophase or macrophase–microphase. Which sequence is preferred can be predicted from the homopolymer–copolymer chain-length ratio.

(Keywords: polymer blends; block copolymers; miscibility; phase separation; phase morphologies)

INTRODUCTION

Various studies in the last 20 years have drawn attention to the complex miscibility behaviour of blends of homopolymers and block copolymers[1–21] (reviews[11,12]). Even in the simplest systems, made of a homopolymer A and a two-block copolymer $\alpha\beta$, where A and α are chemically the same, microphase as well as macrophase separation was observed[1–16]. As a rule of thumb, macrophase separation was found when the length of the chains A exceeded that of the blocks α. Two different theories treat this phenomenon: one by Hong and Noolandi[15], who analysed the transition range of homogeneous and phase-separated blends A/$\alpha\beta$, and the other by Xie *et al.*[16], who analysed aggregation of preformed micelles of $\alpha\beta$. The next section below deals with the basic effects.

In this study, the temperature phase diagrams of blends of PMMA and a symmetric two-block copolymer P(S-*b*-MMA) (S = styrene, MMA = methyl methacrylate) with various chain-length ratios are discussed. The phase diagrams were investigated by transmission electron microscopy. *Figure 1* demonstrates the types of morphology observed. The pure block copolymer has a lamellar structure (*Figure 1a*). The blends feature micellar microphase separation (*Figure 1b*), but also micelle aggregation (*Figure 1c*) and macrophase separation as found in 'normal' blends (*Figure 1d*).

These structures were obtained by film casting with non-selective solvents, which is the easiest method to induce phase separation from an initially homogeneous state. To determine temperature phase diagrams, films were cast at different temperatures.

Polymers and methods are introduced in the third section. An attempt to predict the various types of morphology with the aid of mean-field calculations is made. Phase diagrams and phase structures are then shown and are discussed in the final section.

* To whom correspondence should be addressed

MICROPHASE AND MACROPHASE SEPARATION

Phase-separation morphologies in cast films of blends A/$\alpha\beta$ of a homopolymer A and a two-block copolymer $\alpha\beta$, where A and α are chemically the same and immiscible with β, show, as witnessed by *Figure 1*, some special features not found in blends A/$\alpha\beta'$ with a copolymer $\alpha\beta'$ that has a random comonomer sequence. Blends A/$\alpha\beta'$ can merely produce macrophase structures as shown in *Figure 1d* without, of course, the internal microstructure of the copolymer phase. The differences between block copolymer and random copolymer blends are particularly obvious when the copolymers are symmetric, which for $\alpha\beta$ means equal lengths of the two blocks. When the blocks α and β are truly polymeric, they are much longer than the correlation length of intramolecular interactions. The blocks can thus move out of each other's reach, whereby the copolymer $\alpha\beta$ assumes a microphase-separated structure as seen in *Figure 1a*. By phase-separating, the block copolymer acts as a two-component system. A random copolymer with its short sequences of either monomer cannot do this. It always behaves as a one-component system. Binary blends A/$\alpha\beta$ with a two-block copolymer must thus be assigned three components, while random copolymer blends A/$\alpha\beta'$ have only two.

With three components, blends A/$\alpha\beta$ can have up to three phases, as is illustrated in *Figure 2*. Above, the one-phase system was excluded, which leaves the two-phase and three-phase systems. The micellar structure in *Figure 1b* has two phases. The morphologies in *Figures 1c* and *1d* both have three phases, where the blocks of S and MMA are microphase-separated and, together, macrophase-separated from PMMA.

The three-phase morphologies seem extraordinary. A and α being chemically equal, A–α segregation as indicated in *Figure 2c* should be impossible. Chains A and blocks α, together, should segregate from the blocks β, which amounts only to a micellar two-phase micro-

0032-3861/91/061065-12

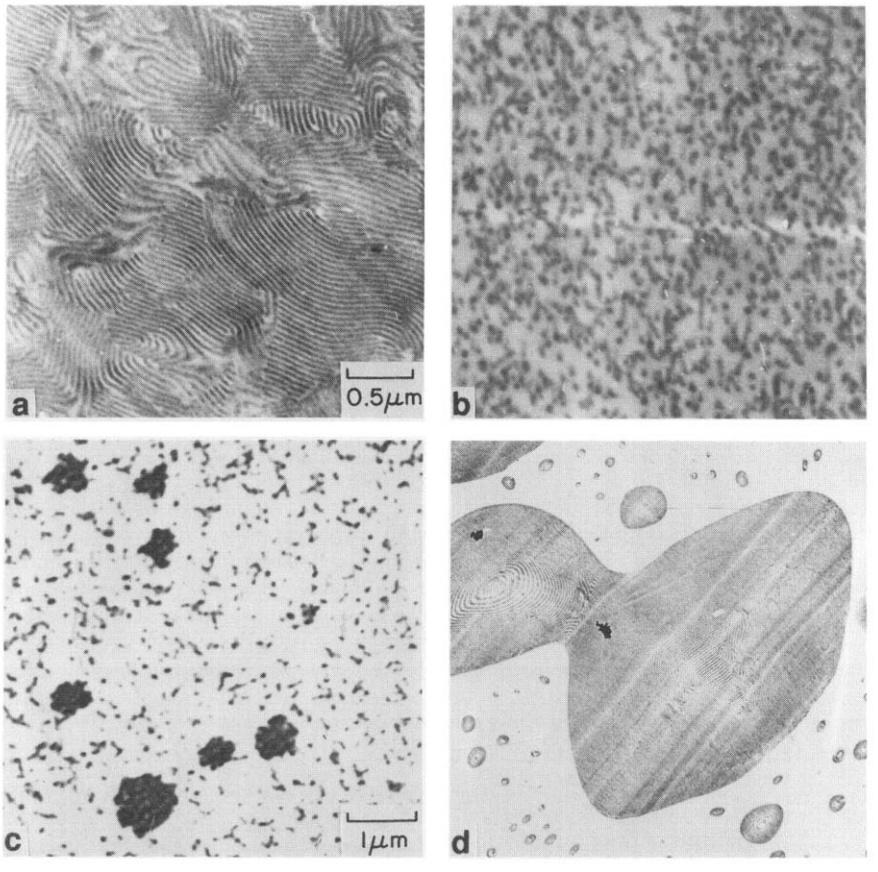

Figure 1 Phase morphologies of (a) a block copolymer P(S-*b*-MMA) and (b)–(d) its blends (copolymer content $f = 0.30$) with PMMA of increasing chain length

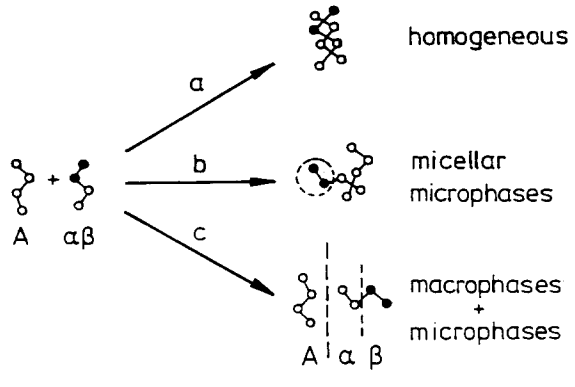

Figure 2 Phase behaviour of a blend A/$\alpha\beta$ of a homopolymer A and a block copolymer $\alpha\beta$

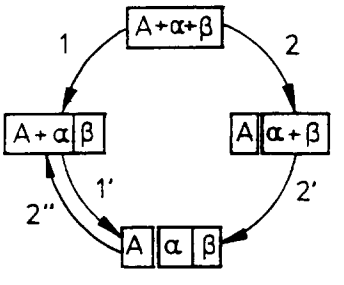

Figure 3 Phase separation during film casting of a blend A/$\alpha\beta$. $A + \alpha + \beta$ is the initial homogeneous solution

structure (*Figure 2b*), as indicated as step 1 in *Figure 3*. There should be no macrophases.

Hong and Noolandi[15] have demonstrated how macrophase separation can nevertheless occur, even without any A–α interaction effects. When A–β incompatibility is stronger than α–β incompatibility, the chains A will reject in the first step of phase separation not only the blocks β but rather the entire copolymer chains $\alpha\beta$, whereby macrophases are formed. Only afterwards, in a second step, will α and β form microphases within the copolymer macrophase. This is sequence $2 + 2'$ in *Figure 3*. The block copolymer $\alpha\beta$ behaves in step 2 like a random copolymer. That it has two blocks shows only in step 2'. The final morphology may look as seen in *Figure 1d*.

This mechanism is analysed in a later section. It does not necessarily describe a complete sequence of processes, since step 2' brings up new effects. When microphases of α and β are formed, A–β encounters are diminished, since the chains A will prefer to have blocks α between them and the blocks β (as indicated in *Figure 2c*). When the α–β microstructure is fully developed, a fur of blocks α covers the microphases of β. A and β are then virtually out of contact and the reason for macrophase separation no longer exists. The three-phase structure in *Figure 1d* should, therefore, go back to the micellar structure shown in *Figure 1b* (step 2" in *Figure 3*).

This suggests that macrophase separation is only an intermediate stage of the sequence $2 + 2' + 2''$ in *Figure 3*, except when α–β incompatibility is weak, or when diffusion is too slow for step 2".

However, microphase formation does not only subdue A–β interaction effects. It also builds up adverse A–α interaction effects not existent in the homogeneous blends, which were analysed by Xie *et al.*[16]. Chains A

and blocks α mix unhindered only in one-phase systems. In micellar two-phase systems, where the blocks α are fixed at the microphase interfaces, A and α can only interpenetrate effectively when they abandon their Gaussian coil statistics. The coils of both are elongated, which can cost sufficient entropy to induce segregation of A and α. This 'A–α effect' can either initiate aggregation of micelles (*Figure 1c*) as indicated by the sequence $1 + 1'$ in *Figure 3*, or it can interrupt the sequence $2 + 2' + 2''$ at $2 + 2'$ and stabilize the macrophases (*Figure 1d*).

A summary in terms of *Figure 3* is that phase separation in cast films of blends A/$\alpha\beta$:

(i) can *start* with microphases (step 1) or with macrophases (step 2), owing to α–β or A–β incompatibility;

(ii) can, *after step 1*, go on to microphase–macrophase structures (sequence $1 + 1'$), owing to the A–α effect; and

(iii) will, *after step 2*, go on to macrophase–microphase structures (sequence $(2 + 2')$, which can go on further to structures with only microphases (sequence $2 + 2' + 2''$), or can persist, owing to either the A–α effect or kinetic hindrance of step $2''$.

MATERIALS AND METHODS

Materials

The polymers and solvents are shown in *Table 1*. Listed are the volume content x of MMA in the copolymers measured by ^{1}H n.m.r. spectroscopy and elemental analysis, the weight-average molecular weight M_w and the polydispersity M_w/M_n obtained from g.p.c. with PMMA and PS calibration. The two-block copolymer P(S-*b*-MMA) was made via anionic polymerization (Polymer Standards Service, Mainz, Germany). The other polymers were made by radical polymerization. In the case of the random copolymer P(S-*co*-MMA) the reaction was stopped at <0.10 conversion to ensure chemical homogeneity. Also listed in *Table 1* are the molecular volume $V_i = M_{wi}/(\rho_i N_A)$, where ρ_i is the density and N_A is Avogadro's number, and for PMMA the chain-length ratio $\lambda = V_A/V_{\alpha\beta}$.

Blend film casting

The blend components were dissolved, in the desired composition f (volume fraction of copolymer in the blend before dissolution) and at a total polymer concentration of 5 g l^{-1}, in toluene or nitrobenzene. Films, 100 μm thick when dry, were cast at constant temperature in Petri dishes in a thermostatted oven under a controlled indirect stream of nitrogen. Solvent evaporation from the solution was stopped at twice the time necessary to evaporate an equal amount of pure solvent. The residual solvent content of $\phi_S \simeq 0.04$ was removed by drying the films for two days each at 60°C and 100°C. Film morphologies could be excellently reproduced.

Phase diagrams were recorded by film casting at different temperatures between 20 and 180°C (with toluene up to 100°C). The casting rate was characterized by the reduced rate $R = (-\dot{V}_S)/V_P$, where $(-\dot{V}_S)$ is the initial loss rate of volume of solvent and V_P is the total volume of polymer[22]. The casting conditions were always kept constant, so that R increased with temperature in proportion to the vapour pressure. To study rate effects, evaporation was sometimes accelerated or slowed down by applying controlled vacuum or covering the Petri dishes with lids.

Electron microscopy

Thin sections (50 nm thick) were cut from the films perpendicularly to their plane with an ultramicrotome. Electron micrographs were taken in transmission, using an Elmiskop 1a (Siemens, München, Germany). Contrast was provided by selective degradation of the PMMA by the electron beam. The electron micrographs proved that the cast films sometimes had a weak orientation parallel to the film plane.

SPINODALS BY MEAN-FIELD APPROXIMATION

Mean-field approximation calculations yield information on homogeneous systems, i.e. in this study on homogeneous blend solutions up to the point of incipient phase separation. The calculations below describe, therefore, only the initiation of the first step, 1 or 2 in *Figure 3*, of phase separation during film casting. Solutions A/$\alpha\beta$/S and A/$\alpha\beta'$/S of a homopolymer A, a symmetric copolymer $\alpha\beta$ (two-block) or $\alpha\beta'$ (random), and a solvent S are discussed.

Correlations of the concentration fluctuations $\delta\phi_i(q)$ and $\delta\phi_j(q)$ of wavevector q in homogeneous multicomponent systems are characterized by structure

Table 1 Polymers and solvents (see text for details)

	x	M_w	$\frac{M_w}{M_n}$	V_i (nm^3)	$\lambda = \frac{V_A}{V_{\alpha\beta}}$
P(S-*b*-MMA)	0.47	175 000	1.04	$V_{\alpha\beta} = 260$	
P(S-*co*-MMA)	0.49	168 000	1.8	$V_{\alpha\beta'} = 250$	
PMMA	0	35 000	2.0	$V_A = 50$	0.19
		95 000	1.9	130	0.50
		161 000	2.0	225	0.87
		188 000	2.2	263	1.0
		535 000	2.0	749	2.9
Toluene		92		$V_S = 0.177$	
Nitrobenzene		123		0.170	

factors:

$$S_{ij}(q) = V\langle\delta\phi_i(q)\delta\phi_j(q)\rangle = \frac{|M|_{ij}}{|M|}(q) \quad (1)$$

This describes the inversion of a matrix M of the second derivatives of the free energy of mixing ΔF:

$$M_{ij}(q) = \frac{1}{VkT}\left(\frac{\partial^2\Delta F}{\partial\phi_i(q)\partial\phi_j(q)}\right)_{V,T} \quad (2)$$

The Ornstein–Zernicke method to set up M is described in the Appendix[23–26].

Equation (1) does not permit calculation of miscibility gaps, but of the corresponding spinodals. The spinodal conditions are:

$$|M(q)| \to 0 \qquad (\partial|M|/\partial q) = 0 \quad (3)$$

which means $S_{ij}(q)_{max} = S_{ij}(q^*) \to \infty$. This defines those states of the system where its dominant fluctuations, having the 'spinodal wavevector' q^* (position of the maximum of $S_{ij}(q)$), grow infinitely large.

The value of q^* is very informative. Stable, periodic microphase morphologies such as that of a block copolymer $\alpha\beta$ result from dominant fluctuations with a finite $q^* > 0$. Unstable, unordered macrophase morphologies as formed by all 'normal' blends like the random copolymer blends $A/\alpha\beta'$ result from dominant fluctuations at $q^* \to 0$ (*Figure 4*).

Miscibility gaps can be calculated directly by the self-consistent theory developed by Hong and Noolandi[15], but spinodals are easier to compute, which recommends their use in complex systems. They are sufficiently close approximations to reveal all typical features of the miscibility gaps themselves.

Below, the general equations for solutions $A/\alpha\beta/S$ and $A/\alpha\beta'/S$ are adapted for the calculation of spinodals of the blend solutions PMMA/P(S-*b*-MMA)/toluene and PMMA/P(S-*co*-MMA)/toluene (*Table 1*) at room temperature. (Indices are A for chains of MMA, α for blocks of MMA, β for styrene, and S for toluene.) The parameters needed are as follows:

Chain length parameters. PMMA, P(S-*b*-MMA) and toluene are given the chain volumes $V_A = \lambda V_{\alpha\beta}$, $V_{\alpha\beta}$ and V_S of *Table 1*. PMMA is assumed to have the ideal Schulz–Flory chain-length distribution, and P(S-*b*-MMA) is assumed to be monodisperse. These are good approximations. The random copolymer P(S-*co*-MMA) is, to render the blends PMMA/P(S-*b*-MMA) and PMMA/P(S-*co*-MMA) directly comparable, *not* given its own chain volume ($V_{\alpha\beta'}$) and its own chain length distribution, but those of P(S-*b*-MMA) ($V_{\alpha\beta}$, monodisperse). Both copolymers are approximated as exactly symmetric ($x = 0.5$), which yields for the volume per block of P(S-*b*-MMA) $V_\alpha = V_\beta = V_{\alpha\beta}/2$.

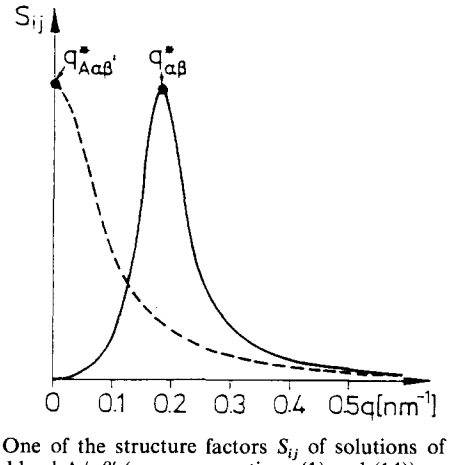

Figure 4 One of the structure factors S_{ij} of solutions of a random copolymer blend $A/\alpha\beta'$ (-----; equations (1) and (14)) and of a pure block copolymer $\alpha\beta$ (———; equations (1) and (18) for $f \to 1$). $q^*_{A\alpha\beta'}$ and $q^*_{\alpha\beta}$ are the 'spinodal wavevectors' of the dominant fluctuations. Solvent concentration ϕ_S was adjusted to yield equal $S_{ij}(q^*)$

Chain stiffness parameters. Instead of the commonly used reduced chain end-to-end distance $(r_i^2/M_i)_w$, the parameter $C_i^2 = (r_i^2/M_i)_w\rho_i N_A$ appears below as the chain stiffness parameter. The actual values are $C^2_{PMMA} = 2.2$ nm^{-1} and $C^2_{PS} = 2.8$ nm^{-1}. The average $C^2 = 2.5$ nm^{-1} is used for all chains and blocks[27] ($C_S^2 \simeq 0$ for toluene).

Interaction parameters. The interaction parameter $\chi = 0.14$ nm^{-3} obtained for the blend PMMA/PS in ref. 28 is used for the interactions between chains or blocks of MMA and styrene in the blend PMMA/P(S-*b*-MMA), and the interactions between chains and blocks of MMA are neglected, so that:

$$\chi_{A\beta} = \chi_{\alpha\beta} = \chi \quad (4)$$

$$\chi_{A\alpha} = 0 \quad (5)$$

The interaction parameter for the blend PMMA/P(S-*co*-MMA) is given by[29–31]:

$$\chi_{A\alpha\beta'} = \chi/4 \quad (6)$$

which is already a result of the model.

Toluene (and nitrobenzene) is a practically non-selective solvent, which prefers neither PMMA nor PS, so that:

$$\chi_{AS} = \chi_{\alpha S} = \chi_{\beta S} = \chi_{\alpha\beta' S} = \chi_S \quad (7)$$

The value $\chi_S = 2.5$ nm^{-3} measured in ref. 28 for room temperature is used. (Note that the Flory–Huggins parameter is $\chi_i^{FH} = V_S\chi_i$.)

The concentration variables of the solutions $A/\alpha\beta/S$ and $A/\alpha\beta'/S$ are the copolymer content f and the solvent concentration ϕ_S.

Solutions $A/\alpha\beta'/S$ (with the random copolymer $\alpha\beta'$)

The matrix is in general:

$$M'_1 = [1/S_S] + \begin{bmatrix} 1/S_A - 2\chi_{AS} & \chi_{A\alpha\beta'} - \chi_{AS} - \chi_{\alpha\beta' S} \\ \chi_{A\alpha\beta'} - \chi_{AS} - \chi_{\alpha\beta' S} & 1/S_{\alpha\beta'} - 2\chi_{\alpha\beta' S} \end{bmatrix} \quad (8)$$

where $[1/S_S]$ is a matrix with equal elements (q is now omitted). The ideal structure factors S_i characterize the correlations of intramolecular fluctuations. They are given by:

$$S_i = \phi_i\langle V_i g_i\rangle_w \quad (9)$$

where $\langle\ \rangle_w$ is the weight average, and g_i is the Debye function:

$$g_i = \frac{2}{x}\left(1 - \frac{1}{x}(1 - e^{-x})\right) \qquad x = R_i^2q^2 = \frac{V_iC_i^2}{6}q^2 \quad (10)$$

where R_i^2 is the squared radius of gyration of the chains ($g_S \simeq 1$ for the solvent).

The solutions in question, PMMA/P(S-*co*-MMA)/toluene, have $\phi_A = (1 - \phi_S)(1 - f)$ and $\phi_{\alpha\beta'} = (1 - \phi_S)f$.

With the average stiffness parameter C^2, $R_i^2 = V_i C^2/6$. The ideal structure factors are:

$$S_A = (1-\phi_S)(1-f)\frac{V_A}{1+\frac{1}{2}R_A^2 q^2} = \frac{(1-\phi_S)(1-f)}{1/(\lambda V_{\alpha\beta}) + \frac{1}{12}C^2 q^2} \tag{11}$$

$$S_{\alpha\beta'} = (1-\phi_S) f V_{\alpha\beta} g_{\alpha\beta} \tag{12}$$

$$S_S = \phi_S V_S \tag{13}$$

Equation (11) results from equation (9) for polymers with an ideal chain length distribution[32]. The matrix for PMMA/P(S-*co*-MMA)/toluene now reads, with equations (6) and (7):

$$M' = [X] + \begin{bmatrix} 1/S_A & \chi/4 \\ \chi/4 & 1/S_{\alpha\beta'} \end{bmatrix} \tag{14}$$

where $[X]$ is a matrix with equal elements $X_{ij} = 1/S_S - 2\chi_S$. It is mainly the second matrix with the polymer parameters, not so much $[X]$, that determines position and shape of the spinodals.

Figure 5 shows the spinodals obtained with equations (3) and (14) at $q^* \to 0$ (where $g_{\alpha\beta} = 1$ in equation (12)). They are of the typical parabolic shape of miscibility gaps of solutions of 'normal' blends*. Since the pure homopolymer and the pure random copolymer cannot phase-separate, the miscibility gaps do not touch the axes $f = 0$ and $f = 1$. This is different for the block copolymer.

Solutions $A/\alpha\beta/S$ (with the two-block copolymer $\alpha\beta$)

The matrix is in general:

$$M = [1/S_S] + \begin{bmatrix} 1/S_A - 2\chi_{AS} & \chi_{A\alpha} - \chi_{AS} - \chi_{\alpha S} & \chi_{A\beta} - \chi_{AS} - \chi_{\beta S} \\ \chi_{A\alpha} - \chi_{AS} - \chi_{\alpha S} & S_\beta/\Delta S - 2\chi_{\alpha S} & \chi_{\alpha\beta} - S_\gamma/\Delta S - \chi_{\alpha S} - \chi_{\beta S} \\ \chi_{A\beta} - \chi_{AS} - \chi_{\beta S} & \chi_{\alpha\beta} - S_\gamma/\Delta S - \chi_{\alpha S} - \chi_{\beta S} & S_\alpha/\Delta S - 2\chi_{\beta S} \end{bmatrix} \tag{15}$$

with $\Delta S = S_\alpha S_\beta - S_\gamma^2$.

The block copolymer is characterized by three ideal structure factors, S_α and S_β for correlations within each block, and S_γ for correlations between the two blocks. A symmetric copolymer needs only two functions, e.g. S_2 for the entire chains and S_1 for each block (equation (9))†:

$$S_2 = S_\alpha + S_\beta + 2S_\gamma = (1-\phi_S) f V_{\alpha\beta} g_2 \tag{16}$$

$$S_1 = S_\alpha = S_\beta = (1-\phi_S)\tfrac{1}{4} f V_{\alpha\beta} g_1 \tag{17}$$

The squared radii of gyration for g_2 and g_1 (equation (10)) are $R_2^2 = V_{\alpha\beta}C^2/6$ for the chain and $R_1^2 = R_2^2/2$ for each block. The structure factor S_2 is identical to $S_{\alpha\beta'}$ for the random copolymer (equation (12)).

The matrix for the solutions PMMA/P(S-*b*-MMA)/toluene is, with the equations (4), (5) and (7):

$$M = [X] + \begin{bmatrix} 1/S_A & 0 & \chi \\ 0 & S_1/\Delta S & \chi + (S_1 - S_2/2)/\Delta S \\ \chi & \chi + (S_1 - S_2/2)/\Delta S & S_1/\Delta S \end{bmatrix} \tag{18}$$

where $[X]$ is defined as in equation (14).

Figure 6a shows the spinodals obtained with equations (3) and (18) with the shortest ($\lambda = 0.19$), a medium ($\lambda = 0.87$) and the longest chained PMMA ($\lambda = 2.9$). The blends are seen to behave below the copolymer content f_0 exactly like the blends with the random copolymer. *Figure 6b* demonstrates that the dominant fluctuations in solutions of PMMA/P(S-*b*-MMA) up to f_0 have the spinodal wavevector $q^* \to 0$, which is the value for macrophase separation. Equation (3) at $q^* \to 0$ is the same for block copolymer and random copolymer blends:

$$|M(q^* \to 0)| = |M'(q^* \to 0)| \tag{19}$$

That the blends PMMA/P(S-*b*-MMA) contain a block copolymer makes a difference only above the transition concentration f_0, where q^* approaches $q^*_{\alpha\beta}$, which characterizes the microstructure of the pure block copolymer itself. For the blend with $\lambda = 2.9$ the transition at f_0 is even discontinuous, i.e. of first order. One can say that f_0 subdivides the composition axis f of blends PMMA/P(S-*b*-MMA) into ranges for macrophase and microphase separation, i.e. for step 1 and step 2 in *Figure 3*.

Figure 7 shows how f_0 varies with λ. When $\lambda > 1$, the larger part of the spinodals is in the 'macro' domain, i.e. $q^* \to 0$. In this entire domain, the blends should macrophase-separate just like the solutions PMMA/P(S-*co*-MMA), provided that the macrophases are stable. Segregation should start with microphases only in the minor 'micro' range above f_0.

These considerations concern the isothermal phase diagrams of blend solutions at room temperature. For the next section, predictions as to the temperature phase diagrams of the dry blends PMMA/P(S-*b*-MMA) and PMMA/P(S-*co*-MMA) are also needed. They are simple. The interaction parameter χ of styrene and MMA is known to increase considerably with temperature[28]. Since all blends PMMA/P(S-*co*-MMA) already have miscibility gaps at room temperature according to *Figure 6*, ever-widening gaps are expected at all higher temperatures. The blends PMMA/P(S-*b*-MMA) are expected to show the same miscibility gaps up to $f = f_0$. More specifically, the predictions are as follows:

(i) The blend with $\lambda = 2.9$ macrophase-separates essentially like the random copolymer blend.

(ii) The blends with $\lambda = 0.19$ or $\lambda = 0.50$ exhibit practically only microphase separation.

(iii) The blends with $\lambda = 0.87$ or $\lambda = 1.0$ prefer macrophase separation when PMMA is the major component and otherwise microphase separation.

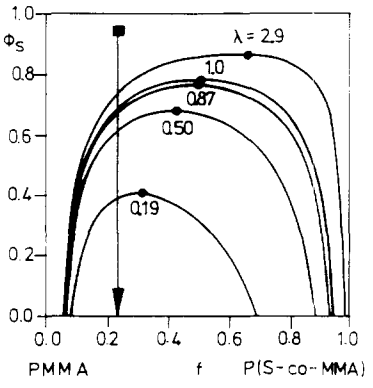

Figure 5 Isothermal phase diagrams of solutions of the random copolymer blends PMMA/P(S-*co*-MMA) by equations (3) and (14). $\lambda = V_A/V_{\alpha\beta}$ is the chain-length ratio. The arrow indicates film casting

* Isothermal phase diagrams for three-component systems are often drawn as equilateral triangles. *Figure 5* is drawn as a square, because this shows the details better

† This holds subject to the condition $C_i^2 = C^2$ for all i

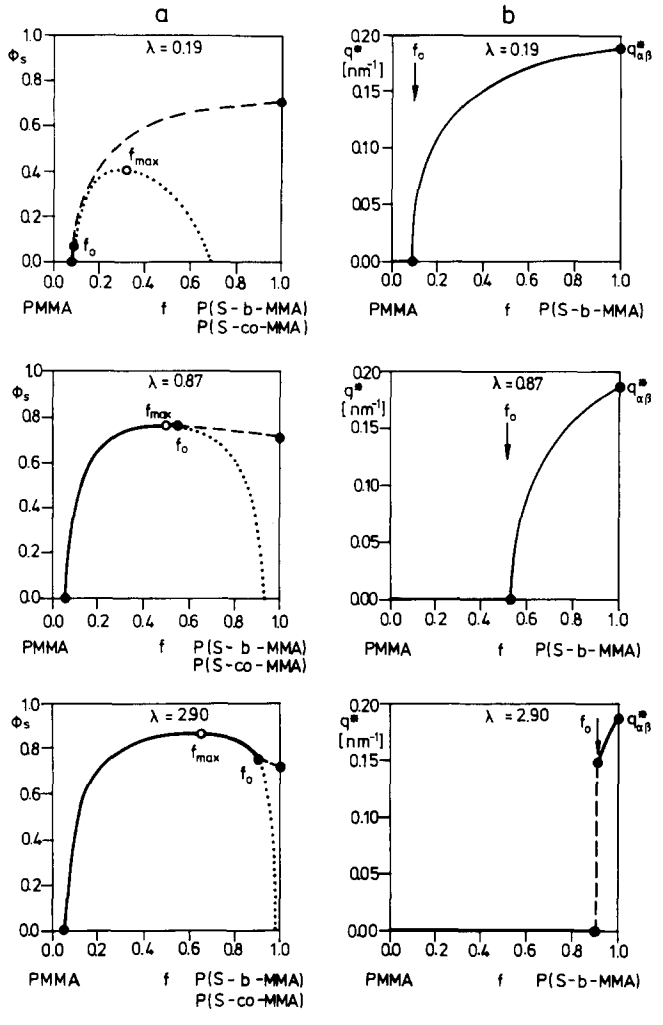

Figure 6 (a) Isothermal phase diagrams of solutions of the block copolymer blends PMMA/P(S-*b*-MMA) by equations (3) and (18): (——) microphase separation (f_0 = transition concentration); (· · · · ·) miscibility gap of the blends PMMA/P(S-*co*-MMA) (f_{max} = position of the maximum). (b) Spinodal wavevector q^* of solutions of blends PMMA/P(S-*b*-MMA) (also by equations (3) and (18)). $q^*_{\alpha\beta}$ is the value for pure P(S-*b*-MMA)

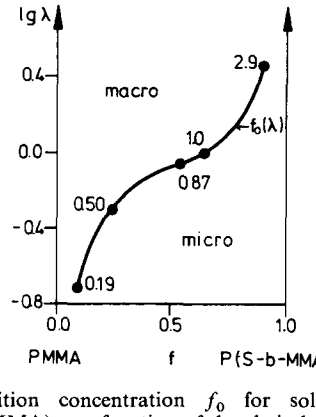

Figure 7 Transition concentration f_0 for solutions of blends PMMA/P(S-*b*-MMA) as a function of the chain-length ratio λ

These predictions were tested in the range of $T \geqslant 20°C$. Note that they refer only to the first step, 1 or 2 in *Figure 3*, of segregation, secondary processes being beyond the scope of the calculations.

PHASE DIAGRAMS AND MORPHOLOGIES

The blends PMMA/P(S-*b*-MMA) with the block copolymer are now described, and in the following subsection they are compared with the corresponding blends PMMA/P(S-*co*-MMA) with the random copolymer.

Blends PMMA/P(S-b-MMA)

Figure 8a shows the temperature phase diagrams of the blends PMMA/P(S-*b*-MMA) as recorded with cast films. The solvents and their rates of evaporation R are indicated. Tests with different rates (10 times faster or slower) reproduced the miscibility gaps within $\pm 10°C$. Exchange of toluene by nitrobenzene below 100°C shifted the miscibility gap of the blend with $\lambda = 0.87$ downwards by 20°C. Solvent and rate effects thus seem small.

Microphase separation prevails almost everywhere in *Figure 8a*, the miscibility gaps indicating only macrophase separation. All gaps are of the low-temperature type with maxima T_{max} shown as a function of λ in *Figure 8b*. This certainly disagrees with the predictions. Closer inspection of the macrophase morphologies in *Figures 9–13* reveals, however, that the predictions are actually not so bad. The different blends behave as follows.

$\lambda = 0.19$ and $\lambda = 0.50$. Segregation starts with and almost always stops at microphase separation. Micellar

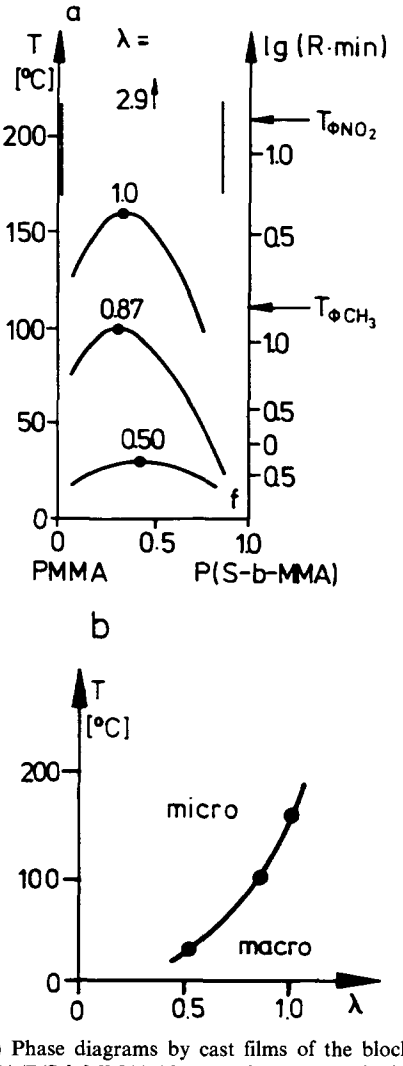

Figure 8 (a) Phase diagrams by cast films of the block copolymer blends PMMA/P(S-*b*-MMA) ($T_{\phi CH_3}$ and $T_{\phi NO_2}$ are the boiling points of the solvents; R is the solvent evaporation rate). (b) Maximum of the miscibility gap as a function of λ

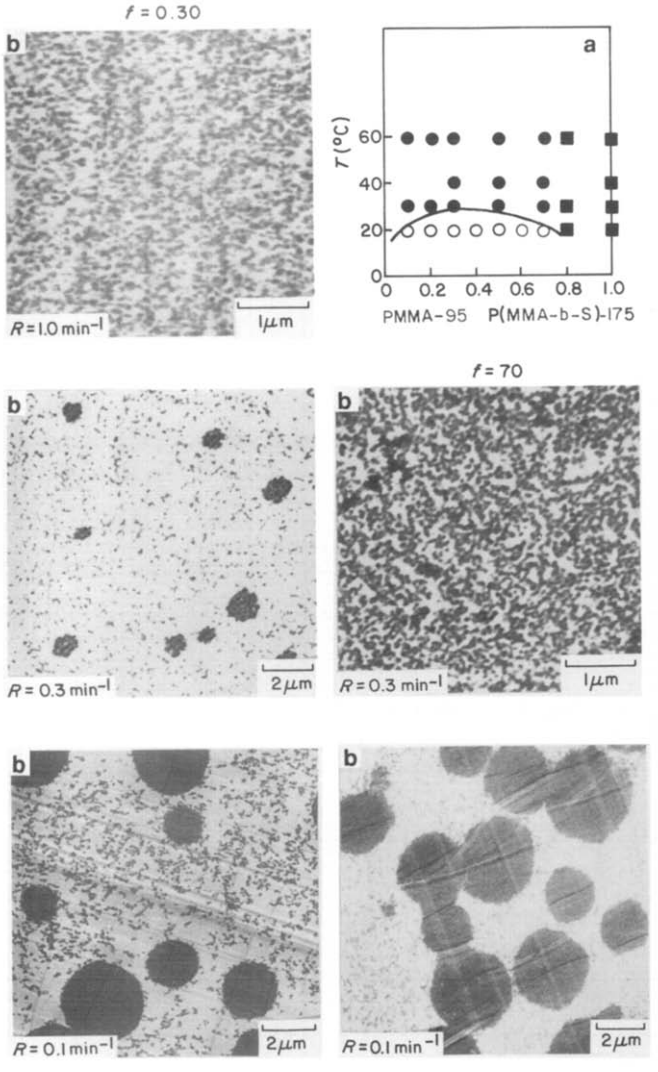

Figure 9 (a) Phase diagram of the blend PMMA/P(S-*b*-MMA) with $\lambda = 0.50$: (●) micelles (as in *Figure 1b*); (■) lamellae (as in *Figure 1a*); (○) micelle aggregates (as in (b)). (b) Micelle aggregation in blends with $f = 0.30$ and $f = 0.70$ at different solvent evaporation rates R

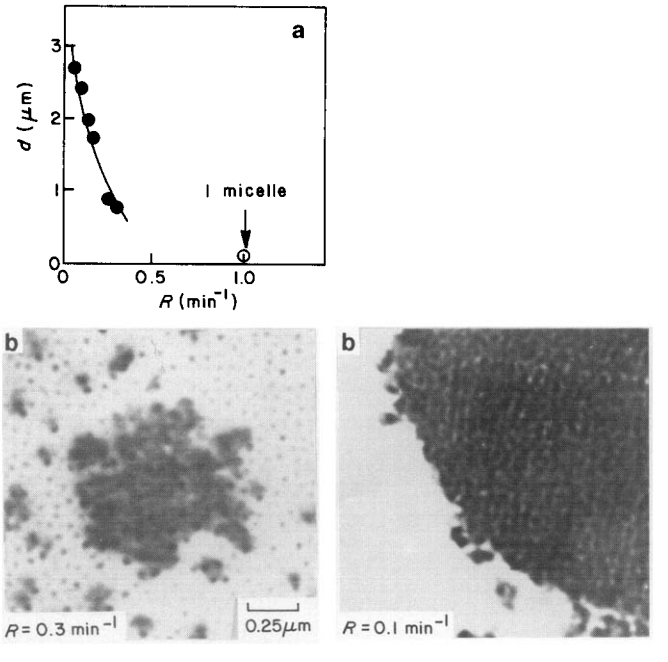

Figure 10 (a) Average diameter d of the micelle aggregates as a function of the evaporation rate R. (b) Micelle aggregates at a high and a low rate R

structures as in *Figure 1b* are formed up to $f \simeq 0.70$, and lamellar structures as in *Figure 1a* from there on. In the present context these micellar morphologies are not of much interest. They are more intriguing in ternary blends PMMA/PS/P(S-*b*-MMA) with both homopolymers, where micelle formation competes with interface stabilization. These blends are discussed in ref. 33.

However, macrophase separation appears, as seen in *Figure 9a*, at room temperature in the blend with $\lambda = 0.50$. It is of the type of micelle aggregation. The pictures for $f = 0.30$ and $f = 0.70$ in *Figure 9b* demonstrate how the tendency towards spherical aggregates of micelles increases as the solvent evaporation rate R is reduced. The domains grow at lower R in size (*Figure 10a*) and perfection (*Figure 10b*).

This type of macrostructure is obviously formed along the sequence $1 + 1'$ in *Figure 3*. Above room temperature segregation stops after step 1.

$\lambda = 0.87$ and $\lambda = 1.0$. Macrophase separation is observed in a substantial part of the temperature interval studied, predominantly in the lower half of the f axis. *Figure 11* shows for the blend with $\lambda = 0.87$ that the macrophases are now not aggregates of micelles. They are rather 'normal' blend morphologies with co-continuous structures in the centre of the miscibility gap, and with island–matrix structures to both sides (see later *Figure 14c*). The structures are larger at lower temperatures; the domain at $T = 20°C$ is already larger than the picture. The copolymer phase always features internal microphase separation. Some PMMA is usually found between the copolymer lamellae (*Figure 12*). Most of it is probably only kinetically trapped. *Figure 13* shows magnifications.

The situation with the blend with $\lambda = 1.0$ is very similar.

Macrophase separation clearly occurs in these blends along the sequence $2 + 2'$ in *Figure 3*. At higher temperatures again only micelles are formed, probably now not via step 1 but via the sequence $2 + 2' + 2''$.

$\lambda = 2.9$. Coarse macrophase morphologies are found at all temperatures and almost all f. A relatively small domain is shown in *Figure 1d*.

In summary, the first two blends start segregation exclusively with microphases, the last three partly or predominantly with macrophases, just as predicted by *Figure 7*. The parameter $f_0(\lambda)$ defines the ranges for preferred segregation along step 1 or step 2 in *Figure 3* quite well. Phase separation indeed starts in a substantial part of the composition axis f with macrophases when $\lambda \geqslant 1$.

The question remains if the macrophase morphologies seen in *Figures 11–13* and in *Figure 1d* owe their persistence to the A–α effect or to kinetic hindrance of step $2''$ of *Figure 3*. The latter possibility cannot readily be ruled out. Lowering the solvent evaporation rate R hardly affected the phase diagrams, but step $2''$ involves redissolution of macrophases, which is a very slow process. At lower temperatures it could be hindered even at extremely low rates. Stabilization of the macrophases by the A–α effect is, nevertheless, more likely. The micelle aggregation (*Figures 9* and *10*) cannot possibly be the product of kinetic effects; it is undoubtedly caused by the A–α effect. *Figure 8b* shows now that T_{max} of this blend and of the others fit very well together. It seems, therefore, straightforward to assume *stabilization of all*

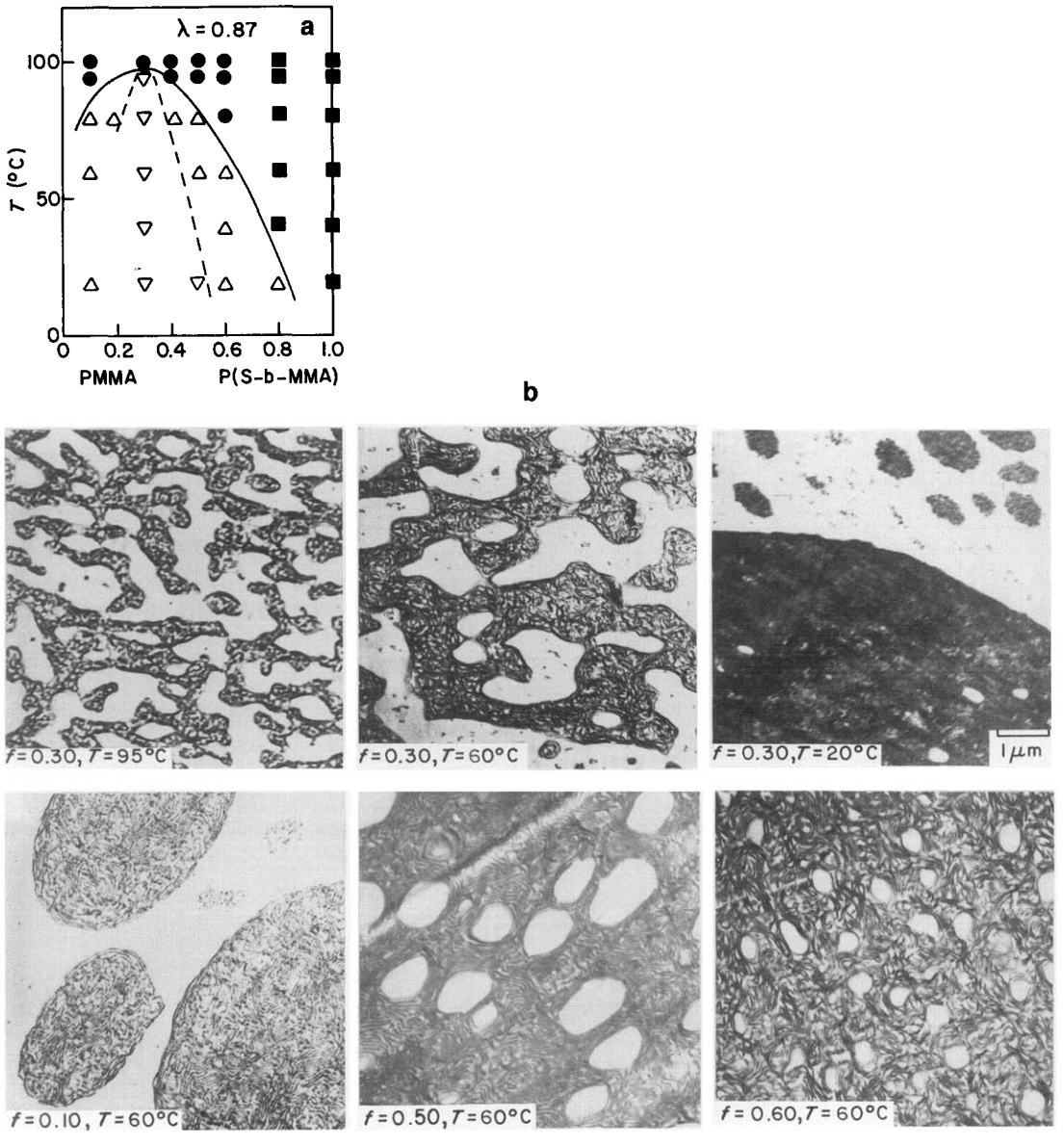

Figure 11 (a) Phase diagram of the blend PMMA/P(S-*b*-MMA) with $\lambda = 0.87$: (●) micelles (as in *Figure 1b*); (■) lamellae (as in *Figure 1a*); (△) island–matrix macrostructures (as $f = 0.10$, 0.50, 0.60 at 60°C in (b)); (▽) co-continuous macrostructures (as $f = 0.30$ in (b)). (b) Macrophase structures of films cast at the rate $R = 0.3\ \text{min}^{-1}$

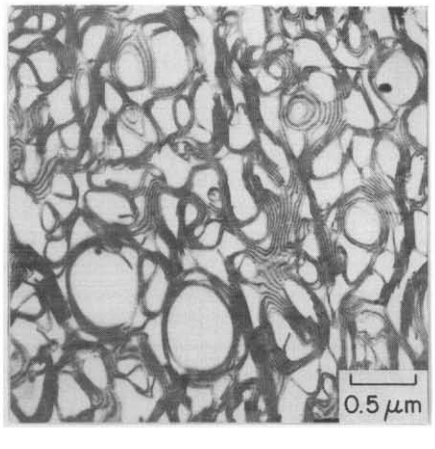

Figure 12 Macrophase structures in a blend film ($f = 0.50$, $T = 60$°C) cast at the high rate $R = 0.1\ \text{min}^{-1}$

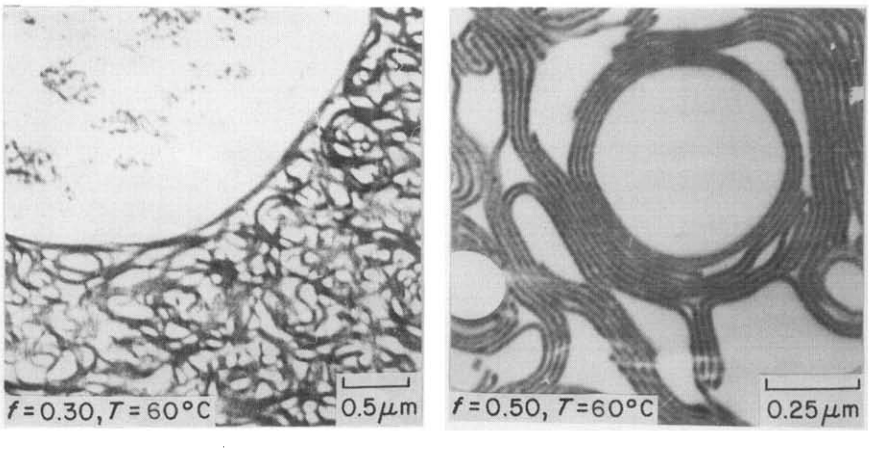

Figure 13 Microstructures within copolymer macrodomains ($T = 60$°C)

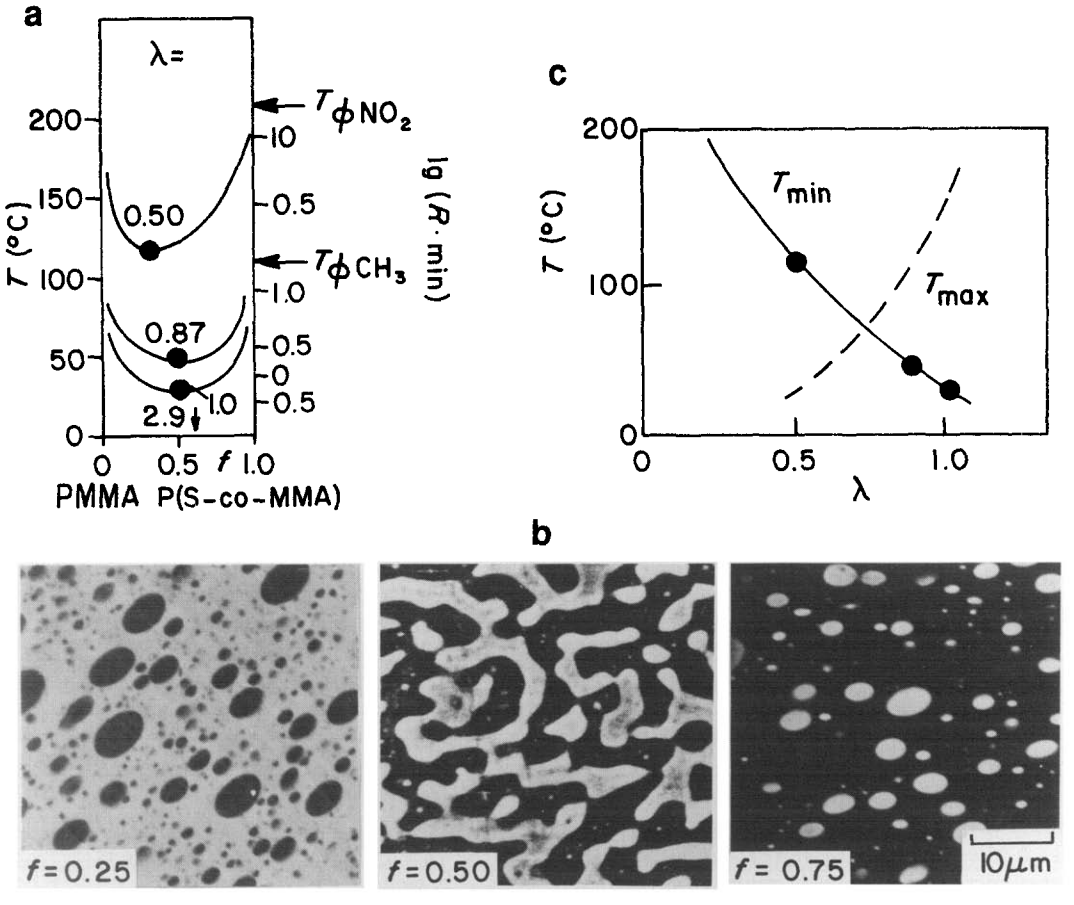

Figure 14 (a) Phase diagrams by cast films of the random copolymer blends PMMA/P(S-*co*-MMA) (as *Figure 8a*). (b) Phase morphologies ($\lambda = 0.87$, $T = 60°C$). (c) Minimum of the miscibility gap as a function of λ; (---) T_{max} of *Figure 8b*

macrophases by the A–α effect. It only remains to explain why this effect loses power at higher temperatures (see conclusions).

Blends PMMA/P(S-co-MMA)

All random copolymer blends PMMA/P(S-*co*-MMA) should have miscibility gaps of the high-temperature type with minima *below* room temperature. *Figure 14a* disproves this. The blends indeed have high-temperature gaps, but all but one end *above* room temperature. The minima T_{min} do not even always overlap with T_{max} of the blends PMMA/P(S-*b*-MMA) (*Figure 14b*). This phenomenon has an explanation. It was discussed in detail in ref. 28. The P(S-*co*-MMA) is actually not the random copolymer meant by the theory in the above section. The point is not the slightly different chain length or the broader chain-length distribution (*Table 1*). The point is that theory always considers for comparison with a two-block copolymer $\alpha\beta$ a random copolymer $\alpha\beta'$ where the short sequences of both monomers behave, in their interactions, like short blocks. Only then has the blend $A/\alpha\beta'$ the interaction parameter $\chi_{A\alpha\beta'} = \chi/4$ (equation (6)). Theory does not recognize that, unlike the block copolymer, the random copolymer has many block junctions and thus many mixed comonomer diads. These perturb the interactions of random copolymers, especially of styrene and MMA, considerably. The blend PMMA/P(S-*co*-MMA) was found to have an interaction parameter about five times lower than $\chi/4$, while that of the blend PS/P(S-*co*-MMA) is not much below χ itself[28].

The real blends PMMA/P(S-*co*-MMA) hence exhibit too much compatibility. If behaving ideally in terms of equation (6), their miscibility gaps would extend to much lower temperatures T_{min}.

CONCLUSIONS

One conclusion from the above is that $f_0(\lambda)$ of *Figure 6* is a rather good parameter to predict the type of segregation, microphase or macrophase, of the first step of phase separation in block copolymer blends PMMA/P(S-*b*-MMA). The mechanism switches between the chain-length ratios $\lambda = 0.50$ and $\lambda = 0.87$. Another conclusion is that, owing to the A–α effect, chains and blocks of MMA segregate at low, but not at high, temperatures. This leads to micelle aggregation in the blend with $\lambda = 0.50$ and to stable macrophases in all blends with $\lambda \geqslant 0.87$.

The summary on blends PMMA/P(S-*co*-MMA) is that, owing to comonomer diad effects, the random copolymer blends PMMA/P(S-*co*-MMA) are not directly comparable with the block copolymer blends, but that 'ideally' behaving blends PMMA/P(S-*co*-MMA), which are comparable, should have miscibility gaps at all temperatures above room temperature.

This suggests a phase diagram for the blend PMMA/P(S-*b*-MMA) with $\lambda = 0.87$ as schematically drawn in *Figure 15*. The transition concentration f_0 for this blend is in the centre of the axis. A high-temperature miscibility gap extending to below room temperature is indicated

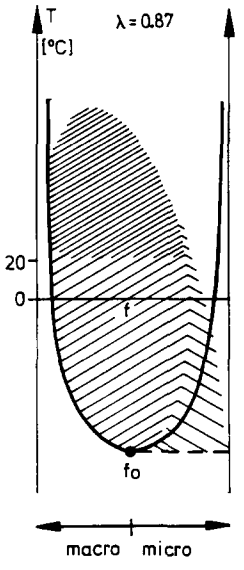

Figure 15 Assumed phase diagram of the blend PMMA/P(S-*b*-MMA) with $\lambda = 0.87$ (see text). //, 'Normal' macrophases; \\, micelle aggregation

for the corresponding 'ideal' random copolymer blend. The low-temperature miscibility gap of the block copolymer blend (*Figure 11a*) is assumed to be part of it. Macrophase separation occurs at lower f, while there may be micelle aggregation at higher f. The effect of another λ on this picture would now mainly be further to decrease (at higher λ) or to widen (at lower λ) the range for micelle aggregation.

The lower part of the figure is, of course, speculative. Similar phase diagrams have been reported by Roe and Zin[7].

What is certain (and, therefore, the conclusion of this study) is that the two different types of macrostructure exist in blends PMMA/P(S-*b*-MMA). *Micelle aggregation* appears only in the range of $\lambda \simeq 0.50$, where A–β incompatibility is not yet sufficient for dominance of macrophase separation, while the A–α effect is already sufficiently strong. Both effects gain power with λ, so that *macrophase separation* as in 'normal' blends dominates when $\lambda \geqslant 1$.

What is not clear is why the A–α effect should lose efficiency at high temperatures. The model by Xie *et al.*[16] considers purely combinatorial entropy contributions to the free energy of mixing ΔF. These arise from the requirements (i) to fill the space in the corona of micelles with segments of A and α so that a constant overall density results, and (ii) to keep chain and block conformations close to Gaussian coil statistics. Temperature should not change this balance. Since the data presented in this study are not suited to elucidate this question, it is left open.

ACKNOWLEDGEMENTS

We should like to thank Dr C. Johann and Dr P. Kilz from Polymer Standards Service (Mainz, Germany) for the preparation and characterization of the block copolymers. Financial support by the Bundesminister für Wirtschaft through the Arbeitsgemeinschaft Industrieller Forschungsvereinigungen e.V. (AIF) is gratefully acknowledged.

REFERENCES

1 Riess, G., Kohler, J., Tournut, C. and Banderet, A. *Makromol. Chem.* 1967, **101**, 58
2 Riess, G. and Jolivet, Y. *Adv. Chem. Ser.* 1975, **142**, 243
3 Inoue, T., Soen, T., Hashimoto, T. and Kawai, H. *Macromolecules* 1970, **3**, 87; in 'Block Copolymers' (Ed. S. Aggarwal), Plenum, New York, 1970, p. 53
4 Eastmond, G. C. and Phillips, D. G. *Polymer* 1979, **20**, 1501
5 Shibayama, M., Hashimoto, T., Hasegawa, H. and Kawai, H. *Macromolecules* 1983, **16**, 1427
6 Zin, W. C. and Roe, R. J. *Macromolecules* 1984, **17**, 183
7 Roe, R. J. and Zin, W. C. *Macromolecules* 1984, **17**, 189
8 Jiang, M., Huang, X. and Yu, T. *Polymer* 1983, **24**, 1259; 1986, **27**, 1923
9 Sardelis, K., Michels, H. J. and Allen, G. *Polymer* 1987, **28**, 244
10 Kinning, D. J., Winey, K. I. and Thomas, E. L. *Macromolecules* 1988, **21**, 3502
11 Aggarwal, S. L. *Polymer* 1976, **17**, 938
12 Roe, R. J. and Rigby, D. *Adv. Polym. Sci.* 1987, **82**, 103
13 Meier, D. *ACS Polym. Prepr.* 1977, **18**, 340
14 Leibler, L., Orland, H. and Wheeler, J. C. *J. Chem. Phys.* 1983, **79**, 3550
15 Hong, K. H. and Noolandi, J. *Macromolecules* 1983, **16**, 1083
16 Xie, H., Liu, Y., Jiang, M. and Yu, T. *Polymer* 1986, **27**, 1928
17 Duplessix, R., Picot, C. and Benoit, H. *J. Polym. Sci., Polym. Lett. Edn* 1971, **9**, 321
18 Hashimoto, H., Fujimura, H., Hashimoto, T. and Kawai, H. *Macromolecules* 1981, **14**, 844
19 Selb, J., Marie, P., Rameau, A., Duplessix, R. and Gallot, Y. *Polym. Bull.* 1983, **10**, 444
20 Rigby, D. and Roe, R. J. *Macromolecules* 1984, **17**, 1778; 1986, **19**, 721
21 Whitmore, M. D. and Noolandi, J. *Macromolecules* 1985, **18**, 657
22 Yu, D., Kohl, P. R. and Hellmann, G. P. *Colloid Polym. Sci.* in press
23 Ornstein, L. S. and Zernicke, T. *Proc. Acad. Sci. Amsterdam* 1914, **17**, 793
24 Leibler, L. *Macromolecules* 1980, **13**, 1602
25 Benoit, H., Wu, W., Benmouna, M., Mozer, B., Bauer, B. and Lapp, A. *Macromolecules* 1985, **18**, 986
26 Mori, K., Tanaka, T. and Hashimoto, T. *Macromolecules* 1987, **20**, 381
27 'Polymer Handbook' (Eds J. Brandrup and E. H. Immergut), Interscience, New York, 1967, Ch. IV
28 Kohl, P. R., Seifert, A. M. and Hellmann, G. P. *J. Polym. Sci., Polym. Phys. Edn* 1990, **28**, 1309
29 Paul, D. R. and Barlow, J. W. *Polymer* 1984, **25**, 487
30 ten Brinke, G., Karasz, J. E. and MacKnight, W. J. *Macromolecules* 1983, **16**, 1827
31 Kambour, R. P., Bendler, J. T. and Bopp, R. C. *Macromolecules* 1983, **16**, 753
32 Benoit, H. *J. Polym. Sci.* 1953, **11**, 507
33 Löwenhaupt, B. and Hellmann, G. P. *Colloid Polym. Sci.* 1990, **268**, 885
34 de Gennes, P. G. 'Scaling Concepts in Polymer Physics', Cornell University Press, Ithaca, NY, 1979

APPENDIX

The Ornstein–Zernicke approach to the analysis of the structure factors S_{ij} of multicomponent systems involving polymers (equation (1)) was analysed by Benoit *et al.*[25]. What follows is a method to set up the matrix M. Blends A/B, block copolymers $\alpha\beta$ and solutions A/$\alpha\beta$/S (equation (15)) are treated. Generalizations are simple. (To render the figures and equations easier to read, the structure factors S_{ij} will appear as h_{ij} $(= S_{ij})$.)

The Ornstein–Zernicke picture for the spatial correlations between fluctuations $\delta\phi_A$ at 0 and 1 is shown in *Figure 16* for a pure polymer A. In this case $\delta\phi_A = \delta V_A/V$ describes the total volume fluctuations or 'density fluctuations'. The spatial pair correlation function:

$$h_{AA}(0, 1) = V\langle\delta\phi_A(0)\delta\phi_A(1)\rangle \qquad \text{(A1)}$$

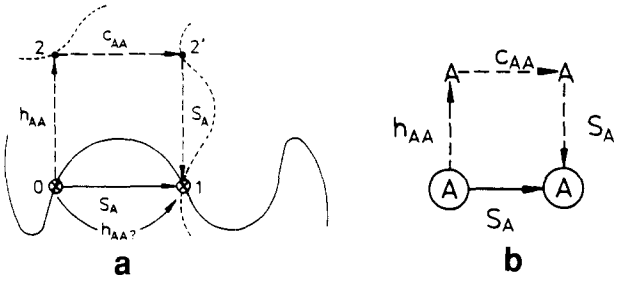

Figure 16 (a) Direct ($0 \rightarrow 1$) and indirect ($0 \rightarrow 2 \rightarrow 2' \rightarrow 1$) correlation between the points 0 and 1 in a pure polymer A. (b) Schematic picture for the correlations A–A

is calculated in a summation scheme. Direct intramolecular correlations (S_A) are due to the probability of chains touching both 0 and 1. Indirect contributions come from the cloud of secondary fluctuations $\delta\phi(2)$ around 0 (h_{AA}). These interact with point 1 first via the intermolecular pair potential (c_{AA}), then via the intrachain correlation (S_A). The total of these indirect effects is the convolution over all paths $0 \rightarrow 2 \rightarrow 2' \rightarrow 1$, so that:

$$h_{AA}(0, 1) = S_A(0, 1) + h_{AA}(0, 2) \otimes c_{AA}(2, 2') \otimes S_A(2', 1) \tag{A2}$$

Fourier transformation yields in wavevector space:

$$h_{AA}(q) = S_A(q)[1 + c_{AA}(q)h_{AA}(q)] \tag{A3}$$

$S_A(q)$ is the ideal structure factor of the chain (equation (9)). Solution of equation (A3) yields:

$$h_{AA} = \frac{1}{1/S_A - c_{AA}} \tag{A4}$$

This equation is only supposed to demonstrate the summation scheme. The one-component system happens to be the one case where the model is inadequate. The interaction function can be split into two terms:

$$c_{AA} = -C + \varepsilon_{AA} \tag{A5}$$

of which the first basically describes the particle–particle repulsions, which dominate the density fluctuations, while the second describes the attractions. Relations for all liquids are:

$$1/S_A \ll |C| \qquad \varepsilon_{AA} \ll |C| \tag{A6}$$

so that equation (A5) is practically:

$$h_{AA} = -1/C \tag{A7}$$

This states correctly that liquids, being almost incompressible, have a low level of density fluctuations. Mean-field considerations, however, break down under the conditions of equation (A6), and equation (A7) is analytically useless.

The Ornstein–Zernicke approach is much better suited to describe systems with two or more components, where $\delta\phi_i = \delta V_i/V$ describes partial volume fluctuations or 'concentration fluctuations' (the density fluctuations being given by $\sum \delta\phi_i$).

Figure 17 shows how *Figure 16* changes when A is mixed with another polymer B. Blends A/B have three correlation functions, h_{AA}, h_{BB} and h_{AB}. There are two paths of indirect correlation, $A \rightarrow A \rightarrow A \rightarrow A$ and $A \rightarrow B \rightarrow A \rightarrow A$, and a scheme for h_{AB} (*Figure 17b*) is needed to calculate h_{AA} (*Figure 17a*). The equations analogous to equation (A3) are:

$$\begin{aligned} h_{AA} &= S_A(1 + c_{AA}h_{AA} + c_{AB}h_{AB}) \\ h_{AB} &= S_B(c_{AB}h_{AA} + c_{BB}h_{AB}) \end{aligned} \tag{A8}$$

which yields:

$$h_{AA} = \frac{S_A(1 - c_{BB}S_B)}{1 - c_{AA}S_A - c_{BB}S_B + (c_{AA}c_{BB} - c_{AB}^2)S_AS_B} \tag{A9}$$

This, and h_{BB} and h_{AB}, can be written as:

$$h_{ij} = |m|_{ij}/|m| \tag{A10}$$

with the 2×2 matrix:

$$m = \begin{bmatrix} 1/S_A - c_{AA} & -c_{AB} \\ -c_{AB} & 1/S_B - c_{BB} \end{bmatrix} \tag{A11}$$

With the subdivision, as in equation (A5):

$$c_{ij} = -C + \varepsilon_{ij} \tag{A12}$$

this reads:

$$m = [C] + \begin{bmatrix} 1/S_A - \varepsilon_{AA} & -\varepsilon_{AB} \\ -\varepsilon_{AB} & 1/S_B - \varepsilon_{BB} \end{bmatrix} \tag{A13}$$

Blends A/B have only two ideal structure factors, S_A and S_B. This is different for block copolymers $\alpha\beta$, which have S_α and S_β, but further S_γ for the block-to-block correlations. This leads to a direct correlation in *Figure 18b*, and to more paths of indirect correlation. The equation analogous to equation (A9) is:

$$h_{\alpha\alpha} = \frac{S_\alpha - c_{\beta\beta}\Delta S}{1 - c_{\alpha\alpha}S_\alpha - c_{\beta\beta}S_\beta - 2c_{\alpha\beta}S_\gamma + (c_{\alpha\alpha}c_{\beta\beta} - c_{\alpha\beta}^2)\Delta S} \tag{A14}$$

with

$$\Delta S = S_\alpha S_\beta - S_\gamma^2 \tag{A15}$$

This, and $h_{\beta\beta}$ and $h_{\alpha\beta}$, is again given by equation (A10) with the 2×2 matrix:

$$m = [C] + \begin{bmatrix} S_\beta/\Delta S - \varepsilon_{\alpha\alpha} & -S_\gamma/\Delta S - \varepsilon_{\alpha\beta} \\ -S_\gamma/\Delta S - \varepsilon_{\alpha\beta} & S_\alpha/\Delta S - \varepsilon_{\beta\beta} \end{bmatrix} \tag{A16}$$

Straightforward generalization leads to the 4×4 matrix for solutions $A/\alpha\beta/S$:

$$m = [C] + \begin{bmatrix} S_\beta/\Delta S - \varepsilon_{\alpha\alpha} & -S_\gamma/\Delta S - \varepsilon_{\alpha\beta} & -\varepsilon_{\alpha A} & -\varepsilon_{\alpha S} \\ -S_\gamma/\Delta S - \varepsilon_{\alpha\beta} & S_\alpha/\Delta S - \varepsilon_{\beta\beta} & -\varepsilon_{\beta A} & -\varepsilon_{\beta S} \\ -\varepsilon_{\alpha A} & -\varepsilon_{\beta A} & 1/S_A - \varepsilon_{AA} & -\varepsilon_{AS} \\ -\varepsilon_{\alpha S} & -\varepsilon_{\beta S} & -\varepsilon_{AS} & 1/S_S - \varepsilon_{SS} \end{bmatrix} \tag{A17}$$

To arrive at the matrices M of equation (2) it must be

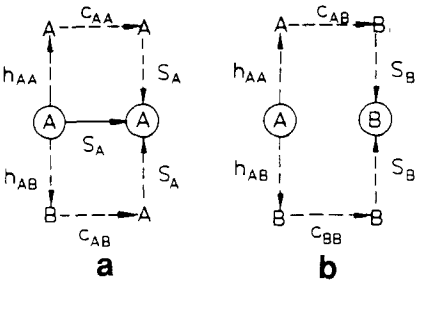

Figure 17 Correlations (a) A–A and (b) A–B in a polymer blend A/B

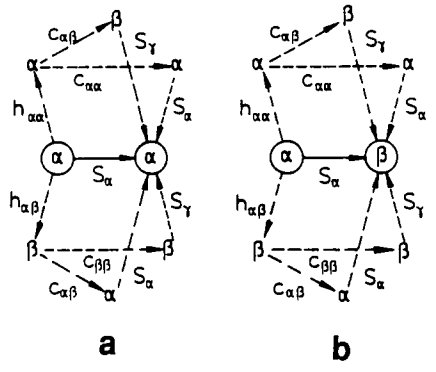

Figure 18 Correlations (a) α–α and (b) α–β in a pure block copolymer $\alpha\beta$

appreciated that the density fluctuations $\sum \delta\phi_i$ in all liquid systems are very small (equation (A7)):

$$\sum_{i,j} h_{ij} = -1/C \simeq 0 \qquad \text{(A18)}$$

which means that:

$$h_{i\omega} = -\sum_{j \neq \omega} h_{ij} \qquad h_{\omega\omega} = \sum_{i,j \neq \omega} h_{ij} \qquad \text{(A19)}$$

where ω is the last component. Matrix m can be lowered in rank by 1, whereby C is eliminated. The resulting matrix is M, with the elements:

$$M_{ij} = m_{ij} + m_{\omega\omega} - m_{i\omega} - m_{j\omega} \qquad i, j \neq \omega \qquad \text{(A20)}$$

In solutions, the solvent S is usually chosen for ω.

When the interaction functions ε_{ij} are combined into interaction parameters as:

$$\chi_{ij} = \tfrac{1}{2}(\varepsilon_{ii} + \varepsilon_{jj} - 2\varepsilon_{ij}) \qquad \text{(A21)}$$

this yields the following:

(i) For blends A/B (equation (A13)):

$$M = \frac{1}{S_A} + \frac{1}{S_B} - 2\chi_{AB} \qquad \text{(A22)}$$

(ii) For block copolymers $\alpha\beta$ (equation (A16)):

$$M = \frac{S_\alpha + S_\beta + 2S_\gamma}{\Delta S} - 2\chi_{\alpha\beta} \qquad \text{(A23)}$$

(iii) For solutions A/$\alpha\beta$/S (equation (A17)) the matrix given in equation (15).

Equation (A22) was first derived by de Gennes[34], equation (A23) by Leibler[24].